A Soluble High Molecular Weight Copolymer of Benzo[1,2-b:4,5-b′]dithiophene and Benzoxadiazole for Efficient Organic Photovoltaics[a]

Wanyi Nie, Christopher M. MacNeill, Yuan Li, Ronald E. Noftle, David L. Carroll, Robert. C. Coffin*

The synthesis and characterization of a soluble high molecular weight copolymer based on 4,8-*bis*(1-pentylhexyloxy)benzo[1,2-*b*:4,5-*b*′]dithiophene and 2,1,3-benzoxadiazole is presented. High efficiency organic photovoltaic (OPV) devices comprised of this polymer and phenyl-C_{71}-butyric acid methyl ester ($PC_{71}BM$) were fabricated by additive processing with 1-chloronapthalene (CN). When the active layer is cast from pristine chlorobenzene (CB), power conversion efficiencies (PCEs) average 1.41%. Our best condition—using 2% chloronapthalene as a solvent additive in CB—results in an average PCE of 5.65%, with a champion efficiency of 6.05%.

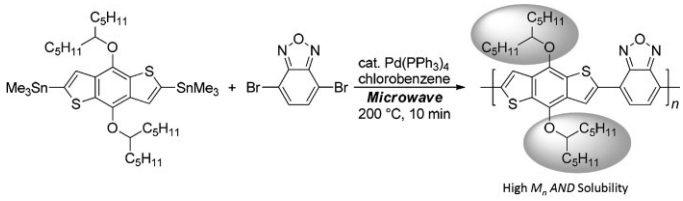

Introduction

The promise of light-weight flexible devices and low cost roll-to-roll processing has attracted a considerable amount of attention to organic photovoltaics (OPVs).[1] These devices have traditionally been plagued by low power conversion efficiencies (PCEs), but over the last few years great improvements in PCEs have been realized. This has been primarily influenced by an influx of new low bandgap polymers[2] that are capable of PCEs much higher than poly(3-hexylthiophene) (P3HT), but also by the development of new processing methods[3] and a better understanding of how processing can affect the bulk heterojunction morphology.[4] However, many new materials, despite having attractive highest occupied molecular orbital (HOMO) and lowest unoccupied molecular orbital (LUMO) levels for OPV applications, suffer from poor device performance. This can be a result of an intrinsic polymer property such as poor hole mobility, but is frequently a result of low molecular weight ($\overline{M}_n$) and poor solubility. High molecular weights are generally required for good OPV performance while good solubility is required for the fabrication of uniform thin films. These properties are often related since precipitation of a poorly soluble polymer during polymerization will limit $\overline{M}_n$ growth.

A particularly interesting class of copolymers are those based on benzo[1,2-b:4,5-b′]dithiophene. There have now been several reports of BDT copolymers exceeding 6% PCE, indicating that BDT has great potential as a building block for OPV donor materials.[5] However, several BDT copolymers have been reported that show low PCEs, including a series of materials reported by Hou et al.[6] Employing 4,8-didodecyloxy-BDT as a comonomer, they report several low

R. C. Coffin, W. Nie, Y. Li, D. L. Carroll
The Center for Nanotechnology and Molecular Materials and the Department of Physics, Wake Forest University, Winston Salem, North Carolina 27109, USA
E-mail: coffinrc@wfu.edu
C. M. MacNeill, R. E. Noftle
The Department of Chemistry, Wake Forest University, Winston Salem, North Carolina 27109, USA

[a] **Supporting Information** for this article is available from the Wiley Online Library or from the author.

DOI: 10.1002/marc.201100161

bandgap copolymers including one based on the common acceptor monomer benzothiadiazole (BT). This polymer, referred to as **H7** was found to have a PCE of 0.90%. Subsequent reports of BDT copolymers have indicated that linear alkoxy chains at the 4- and 8-positions of BDT result in poorly processable low molecular weight ($\overline{M}_n$) materials.[5a,7] We thus expected that PCEs of BDT donor acceptor copolymers, such as **H7** could be improved by transitioning to a branched side chain to enhance $\overline{M}_n$ and solubility. We further envisioned that using benzoxadiazole (BO) as an acceptor monomer instead of BT could lead to PCE improvements. BO has been shown to lead to deeper HOMO levels, which in-turn leads to increased open circuit voltages (V_{oc}) in OPVs.[8] Initially, we tried to synthesize copolymers of BO with the previously reported 4,8-didodecyloxy-BDT and with 4,8-*bis*(2-ethylhexyloxy)-BDT monomers. Both copolymers were intractable. This was surprising given the numerous reports of the solubilizing ability of the 2-ethylhexyl side chain. We then moved to the bulky side chain 1-pentylhexyloxy (see Figure 1a). Unlike 2-ethylhexyloxy, 1-pentylhexyloxy is symmetric, but since the branch is larger and has been moved in one position relative to the polymer backbone, one would expect the bulkiness of this side chain to frustrate aggregation thereby enhancing solubility. This ensures that a higher $\overline{M}_n$ material can be obtained which is beneficial to OPV performance, but in the solid state this frustrated aggregation may impede charge transport.

Experimental Section

Detailed synthetic procedures can be found in the Supporting Information. UV–Vis absorption spectra were recorded on an Agilent 8453 diode-array spectrophotometer operating over a range of 190–1 100 nm. GC–MS were recorded on an Agilent 6850 Series GC system coupled to an Agilent 5973 mass selective detector run in electron impact mode. Thermogravimetric analysis (weight between 10 and 20 mg) was performed under argon (40 mL · min^{-1}) at a rate of 10 °C · min^{-1} from 40–700 °C using a Perkin-Elmer Pyris 1 TGA system. Gel permeation chromatography (GPC, 135 °C in 1,2,4-trichlorobenzene) was performed by American Polymer Standards (Ohio). Tapping mode atomic force microscopy (AFM) images were taken using a JEOL JSPM-5200 AFM. Cyclic voltammetry (CV) was carried out using a computer-controlled Pine Model AFCBP 1 Bi-Potentiostat with PineChem software in a standard single-compartment, three electrode cell. The working electrode was glassy carbon, while the counter electrode was a platinum wire. The pseudo-reference electrode was a silver wire and was calibrated against (Fc/Fc^+). The polymer was drop-cast onto glassy carbon from a 2.5 mg · mL^{-1} solution in chlorobenzene (CB). All measurements were carried out in degassed solutions of acetonitrile with tetrabutylammonium hexafluorophosphate (0.1 M, electrochemical grade) as the supporting electrolyte. The scan rate used was 50 mV · s^{-1}. Highest occupied energy levels (HOMO) and lowest unoccupied energy levels (LUMO) were calculated using Equation (1 and 2):[9]

$$E_{HOMO} = -(E^{ox}_{onset} + 4.8)(eV) \quad (1)$$

$$E_{LUMO} = -(E^{red}_{onset} + 4.8)(eV) \quad (2)$$

X-ray powder diffraction data were collected at room temperature using a BRUKER P4 general-purpose four-circle X-ray diffractometer modified with a GADDS/Hi-Star detector at 40 kV and 30 mA for Cu Kα radiation ($\lambda = 1.5\,406$ Å). The GADDS software suite was used to control the goniometer.[10] The samples were mounted on a loop and two frames were measured at $2\theta = 20$ and 50° with exposure time of 180 s · frame^{-1}. Area integration techniques were used to reproduce the single powder diffraction pattern for each frame. The powder patterns were each merged and analyzed using the EVA program to produce a single powder diffraction pattern.[11]

Photovoltaic devices were fabricated as follows. ITO covered glass (purchased from Delta $R = 8$–10 Ω · sq^{-1}) was cut into 2.5 cm × 2.5 cm chips. The chips were covered by a strip of acid-resistive tape (width ≈1.5 cm), then the ITO was removed from the exposed area by etching with hydrochloric acid (ACS reagent, 37%, Sigma–Aldrich). The resultant chip was cleaned for 15 min in an ultra-sonication bath with Triton X-100, distilled water, acetone, and isopropanol. After drying in a vacuum oven for 1 h, the chips were exposed to ultraviolet ozone plasma for

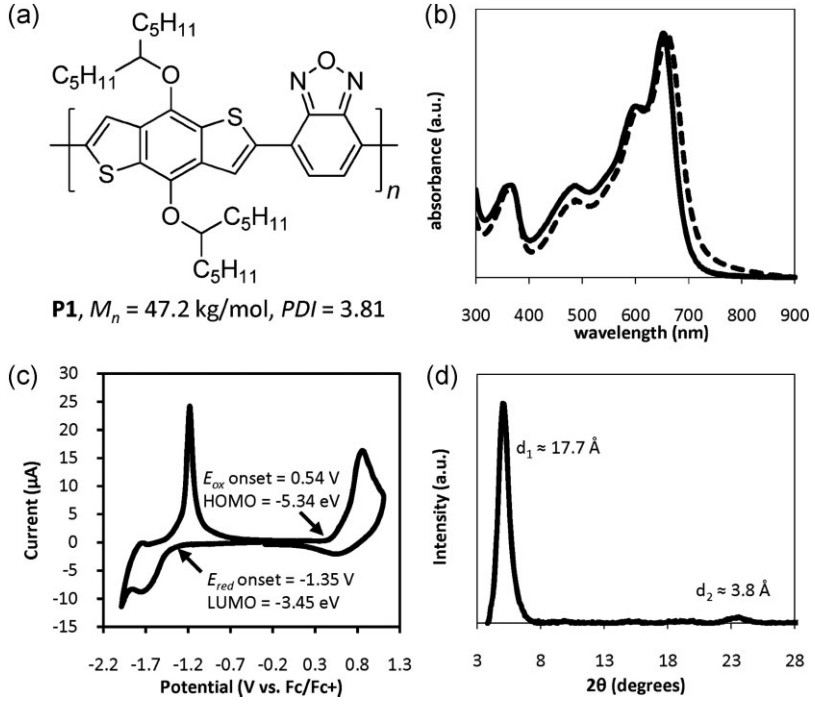

Figure 1. (a) The chemical structure of P1. (b) Chlorobenzene solution (solid line) and film cast from chlorobenzene (dotted line) UV–Vis absorption spectra of P1. (c) Cyclic voltammagram of P1 film. (d) X-ray diffraction patterns of powdery P1.

30 min. A PEDOT:PSS (≈40 nm, CLEVIOS PH 500) film was spin-casted at 4 000 rpm on top of the ITO substrates and dried in a vacuum oven for 10 min at 100 °C. These substrates were then transferred into a nitrogen filled glovebox for active layer deposition. To determine the optimal **P1**:phenyl-C_{71}-butyric acid methyl ester ($PC_{71}BM$) ratio a series of solutions containing 8 mg · mL^{-1} polymer dissolved in 1,2-dichlorobenzene (DCB) with five weight ratios of $PC_{71}BM$ (1:1, 1:1.5, 1:1.8, 1:2, 1:2.2) were spin-casted on top of the PEDOT:PSS. Once dry, the devices were removed from the glovebox then transferred to a thermal-evaporator pump where a thin layer lithium fluoride (0.25 nm) and aluminum cathode (100 nm) were deposited. The active area, which is the area of overlap between the ITO and aluminum strip, were determined by Vernier calipers (0.1 mm, Scienceware) under 10× optical microscope. Each device area was individually determined and ranged in size from 8 to 12 mm^2. Using the optimal **P1**:$PC_{71}BM$ ratio of 1:1.5, solvent processing was explored using the same device architectures. Devices were prepared from (i) CB, (ii) DCB, (iii) CB with 1, 2, and 4% v/v 1-chloronapthalene (CN), (iv) DCB with 1 and 2% CN. The solutions were stirred overnight then heated to 110 °C on a hotplate for 2 h immediately prior to spin-coating. The active layer was deposited using the optimized speed at 1 300 rpm for 30 s. The film dried within 5 min and was transferred to the evaporator for cathode deposition. Film thicknesses were determined by scratching across the film between the cathodes and scanning by AFM (see Figure S5). After subtracting the thickness of the PEDOT:PSS layer, the active layer thicknesses ranged from 100 to 120 nm. All the devices were tested in air using an Oriel 150 W Xenon lamp with AM1.5 g standard filters operating at an illumination intensity of 100 mW · cm^{-2}. Current–voltage characteristics were measured using a Keithley 236 source-measurement unit. At least eight devices were measured under each condition. The external quantum efficiency (EQE) was measured on a Newport Merlin lock-in amplifier by shining a Newport 300 W Xenon light source through a Newport Cornerstone 260 Monochromator. EQE was determined by comparison with a NIST calibrated silicon photodiode.

Results and Discussion

P1 was synthesized by microwave-assisted Stille coupling,[12] starting from 2,6-*bis*(trimethyl)-4,8-bis(1-pentylhexyloxy)benzo[1,2-b:4,5-b′]dithiophene and 4,7-dibromo-2,1,3-benzox-adiazole using *tetrakis*(triphenylphosphine)-palladium(0) as a catalyst (see Supporting Information for monomer and polymer synthetic details). The precipitated polymer was transferred to a Soxhlet extractor where it is washed with methanol, hexane, and THF, then extracted with chloroform. The chloroform fraction was filtered through celite to remove palladium,[5a] precipitated in methanol, collected by centrifugation, and dried in vacuo. The resultant material was soluble at >10 mg · mL^{-1} at room temperature in chlorinated aromatic solvents and found to have a number average molecular weight ($\overline{M}_n$) of 47.2 kg · mol^{-1} and a polydispersity index (PDI) of 3.81 (GPC, 135 °C in 1,2,4-trichlorobenzene). This PDI is much higher than the anticipated PDI near 2 for a step-growth polymerization; this may be a result of aggregation of the polymer in TCB solution. UV–Visible spectroscopy of **P1** (Figure 1b) in CB solution reveals λ_{max} at 653 nm, while in the film λ_{max} is slightly red-shifted to 658 nm. The onset of absorption in the film is at ≈740 nm, giving an optical bandgap of ≈1.68 eV. The HOMO and LUMO energy levels were estimated from CV, shown in Figure 1c. The onsets of oxidation and reduction were estimated to be 0.54 and −1.35 V relative to ferrocene (Fc/Fc^+), respectively, giving rise to a HOMO of −5.34 eV and a LUMO of −3.45 eV. As anticipated the HOMO level of **P1** is deeper than that of related BDT-BT copolymer[6] **H7**, while the optical bandgaps are similar, consistent with the relationship between BO and BT copolymer seen elsewhere.[8] The powder X-ray diffraction spectrum shown in Figure 1d shows that the d_1-spacing, corresponding to the in-plane spacing between polymer backbones, is 17.7 Å. This is comparable to 4,8-*bis*(2-ethylhexyloxy)BDT copolymers, an expected result since this spacing is related to side chain length. A low intensity peak at $2\theta = 23.6°$ corresponding to a d_2-spacing (π-stacking distance) of 3.8 Å is also observed. This is larger than is seen for other BDT copolymers ($d_2 \approx 3.6$ Å) owing to the bulk of the 1-pentylhexyloxy side chain. Thermal gravimetric analysis reveals that **P1** is stable to nearly 300 °C similar to **H7**.

For determination of the PV characteristics of **P1**, we used a standard architecture of ITO/PEDOT:PSS/**P1**:$PC_{71}BM$/LiF/Al. $PC_{71}BM$ was used instead of $PC_{61}BM$ because it enhances the absorption in the sub 530 nm range in the active layer, while the LiF hole-blocking layer was used because it was found early-on in our study to improve V_{oc}'s by ≈0.06 V. The devices were fabricated in a glove-box and tested in air. Using DCB as the solvent **P1**:$PC_{71}BM$ ratios were varied from 1:1 to 1:2.2. Figure 2a and b summarize the results with each data point representing the average of at least eight devices, while Figure 2c and d, respectively, show the best current–voltage and EQE curves for each condition. The open circuit voltages (V_{oc}) and fill factors (FF) are relatively constant at ≈0.92 V and 0.48, respectively, at **P1**:$PC_{71}BM$ ratios of 1:1.5 or greater. For a ratio of 1:1.5, the current density (J_{sc}) peaks at ≈7.3 mA · cm^{-2} and the PCE peaks at an average of 3.06%. The V_{oc} is >0.2 V higher for devices fabricated from **P1** when compared to Hou et al's **H7**, consistent with a deeper HOMO level as determined by CV. Using this optimal **P1**:$PC_{71}BM$ ratio, we also processed devices from CB. Despite V_{oc}'s and *FF*'s improving to ≈0.97 V and 0.55, respectively, a precipitous drop in J_{sc} to 2.64 mA · cm^{-2} results in lower average PCE's of ≈1.41%. For devices processed from both CB and DCB thermal annealing resulted in slightly lower device performance.

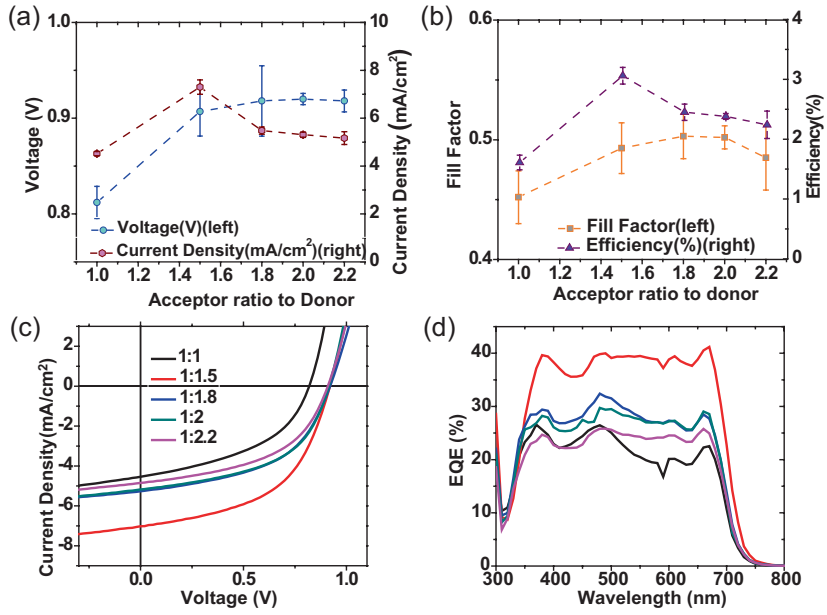

Figure 2. The influence P1:PC71BM ratio on device performance. (a) Summary of open circuit voltage and short circuit current density. (b) Summary of fill factor and power conversion efficiency. Points represent the average of at least eight devices with standard deviations. (c) The best current–voltage curves, and (d) the best external quantum efficiency curves for each condition.

Atomic force microscopy was used to characterize the surfaces of the devices cast from CB and DCB. The images were taken in air on an area between the cathodes. As seen in Figure 3a and b, the topography reveals that the DCB device has larger elevated features and a higher root mean square (RMS) roughness of 7.96 nm compared to the devices processed from CB (RMS roughness of 4.05 nm). This can be correlated to greater phase separation in the DCB devices, likely a result of the slower drying time for the DCB devices (DCB boiling point 180 °C, CB boiling point 131 °C).[13]

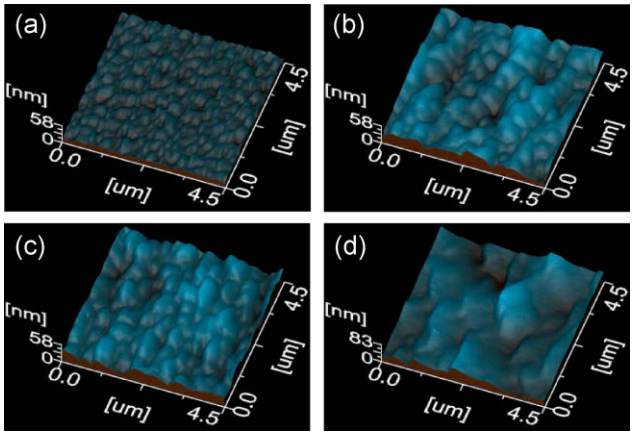

Figure 3. AFM topographic view of active layer spin-casted from (a) chlorobenzene, (b) 1,2-dichlorobenzene, (c) chlorobenzene with 2% 1-chloronaphthalene, and (d) 1,2-dichlorobenzene with 1% 1-chloronaphthalene.

To further improve device performance we investigated additive processing.[14] Two such additives that have been shown to greatly improve device performance are 1,8-diiodooctane ((DIO)[3b] and CN.[8c] Both additives are high boiling and slow the film drying process. However, it has been shown in the literature that they differ in that DIO has been shown to promote polymer aggregation—increasing the domain sizes within the film,[3b] while CN has been shown to prevent polymer aggregation and decrease phase separation.[15] It is worth noting that this is likely highly dependent upon the system being studied and how the processing is performed. Given **P1**'s high solubility and poor tendency to aggregate, we initially investigated DIO as an additive in both CB and DCB. However, DIO processing led to poorly reproducible device performance.

The effects of CN depended greatly on the host solvent. A comparison of the PV characteristics of devices prepared from pristine CB and DCB with those prepared with CN additive is shown in Figure 4a and b, while the best *J–V* and EQE curves for each condition are shown in Figure 4c and d. Using DCB as the host solvent, devices were fabricated from solutions containing 1% (Figure S6a) and 2% CN (Figure 4). Both loadings resulted in a decrease in average device PCE from 3.06% without additive to 2.42% with 1% CN and 1.82% with 2% CN. When CB is used as the host solvent the effect of the additives are quite different. Average PCEs for devices prepared from CB solution without additive was 1.41%. The addition of 1, 2, and 4% CN results in average PCEs of 2.82, 5.65, and 4.01%, respectively (1 and 4%, see Figure S6b, 2% Figure 4). The best device fabricated using 2% CN in CB showed a V_{oc} of 0.887 V, J_{sc} of 13.6 mA · cm^{-2}, FF of 0.508, and PCE of 6.05%. The improvements in PCEs upon addition of CN to CB are a result of dramatically improved J_{sc} from an average of 2.64 mA · cm^{-2} for pristine CB to an average of 12.43 mA · cm^{-2} for CB with 2% CN. For both host solvents, the V_{oc} and *FF* drop upon addition of the CN. A loss in V_{oc} is not uncommon with additive processing,[3a] which is presumably a result of increased ordering stabilizing the HOMO level of the polymer. However, increases in J_{sc} are typically accompanied by increases in FF; a result of improvements in active layer morphology that allow for improved charge separation and collection. The EQE for the best device fabricated from CB with 2% CN is above 55% from 350 to 670 nm reaching a maximum of 69% at 590 nm. The integration of this EQE gives a J_{sc} of 13.1 mA · cm^{-2}; a

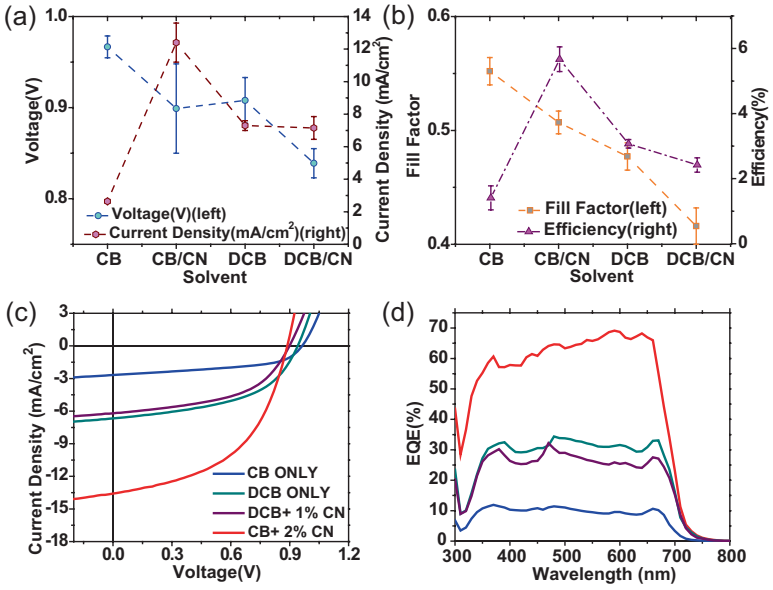

Figure 4. Summary of CN ratio on device performance. (a) Summary of open circuit voltage and short circuit current density. (b) Summary of fill factor and power conversion efficiency. Points represent the average of at least eight devices with standard deviation. (c) The best current–voltage curves, and (d) the best external quantum efficiency curves for each condition.

3.7% error. Since our devices were not encapsulated and measured in air, we attribute this discrepancy to degradation that occurs between making the *J*–*V* and EQE measurements.

Atomic force microscopy topography images of the devices fabricated from DCB with 1% CN and CB with 2% CN are shown in Figures 3c and d, respectively. A comparison of these images with those for the devices prepared from pristine DCB or CB (Figure 3a and b) reveal that additive processing results in a rougher surface and larger domain sizes. The RMS roughness increases from 7.96 to 10.4 nm for the DCB devices and from 4.05 to 7.83 nm for the CB devices. This is opposite to what has been seen previously for CN processed films.[8b] Additionally, upon adding 2% CN to CB, the domain size increases from ≈0.2 to ≈0.4 μm, while the addition of 1% CN to DCB increases the domain sizes from ≈0.4 to ≈1 μm. Relative to the smoothest films prepared from pristine CB, the rougher films resulting from the other processing conditions give lower *FF*'s, but much higher J_{sc}'s resulting in higher *PCE*'s. However, the increase in roughness and domain size is only beneficial to a point as shown by the drop in PCE for the roughest films (produced from DCB with 1% CN). Interestingly, despite very similar topographic images, the films prepared from pristine DCB and CB with 2% CN lead to devices with PCEs that differ by greater than 2%—most likely a result of morphological differences not detectable by AFM.

Conclusion

In summary, we report on the synthesis, characterization, and device performance of poly[4,8-bis(1-pentylhexyloxy)-benzo[1,2-*b*:4,5-*b*′]dithiophene-2,6-diyl-*alt*-2,1,3-benzoxadiazole-4,7-diyl]. The bulky 1-pentylhexyloxy side chain frustrates aggregation, enabling the production of a high molecular weight freely soluble copolymer. OPV devices were fabricated using **P1** in combination with $PC_{71}BM$. At an optimized **P1**:$PC_{71}BM$ ratio of 1:1.5, solvent additive processing was used to further improve device performance. Using DCB as the host solvent, the addition of CN resulted in a decrease in PCE relative to devices prepared from pristine solvent. Conversely, devices prepared from a solution of 2% CN in CB resulted in a dramatic improvement in PCE to an average of 5.65%, compared with 1.41% from pristine CB. The optimized devices have high V_{oc}, and among the highest EQE reported for a low bandgap polymer, but a FF that hovers near 0.5 limits the overall PCE of these devices. We attribute the low FF's to poor packing, a consequence of using the bulky 1-pentylhexyl side chain. It is important to note that four batches of **P1** were used over the course of this work with no discernable batch-to-batch variation in performance.

Acknowledgements: This work was supported by grants from FiberCell Inc. and the Department of Energy (DOE DE-FG02-07ER46428).

Received: March 15, 2011; Revised: May 1, 2011; Published online: June 10, 2011; DOI: 10.1002/marc.201100161

Keywords: conjugated polymers; photovoltaics; synthesis

[1] [1a] W. Cai, X. Gong, Y. Cao, *Sol. Energy Mater. Sol. Cells* **2010**, *94*, 114; [1b] S. Gunes, H. Neugebauer, N. S. Sariciftci, *Chem. Rev.* **2007**, *107*, 1324.
[2] Y.-J. Cheng, S.-H. Yang, C.-S. Hsu, *Chem. Rev.* **2009**, *109*, 5868.
[3] [3a] J. Peet, J. Y. Kim, N. E. Coates, W. L. Ma, D. Moses, A. J. Heeger, G. C. Bazan, *Nat. Mater.* **2007**, *6*, 497; [3b] J. K. Lee, W. L. Ma, C. J. Brabec, J. Yuen, J. S. Moon, J. Y. Kim, G. C. Bazan, A. J. Heeger, *J. Am. Chem. Soc.* **2008**, *130*, 3619; [3c] J. Peet, C. Soci, R. C. Coffin, T. Q. Nguyen, A. Mikhailovsky, D. Moses, G. C. Bazan, *Appl. Phys. Lett.* **2006**, *89*, 252105; [3d] Y. Kim, A. S.

Choulis, J. Nelson, D. D. C. Bradley, *Appl. Phy. Lett.* **2005**, *86*, 063502; [3e] F. Padinger, R. S. Rittberger, N. S. Sariciftci, *Adv. Funct. Mater.* **2003**, *13*, 85.

[4] [4a] M. Campoy-Quiles, T. Ferenczi, T. Agostinelli, P. G. Etchegoin, Y. Jim, T. D. Anthopoulis, P. N. Stavrinou, D. D. C. Bradley, J. Nelson, *Nat. Mater.* **2008**, *7*, 158; [4b] J. S. Moon, C. J. Takacs, S. Cho, R. C. Coffin, H. Kim, G. C. Bazan, A. J. Heeger, *Nano Lett.* **2010**, *10*, 4005.

[5] [5a] Y. Liang, D. Feng, Y. Wu, S.-T. Tsai, G. Li, C. Ray, L. Yu, *J. Am. Chem. Soc.* **2009**, *131*, 7792; [5b] J. Hou, H.-Y. Chen, S. Zhang, R. I. Chen, Y. Yang, Y. Wu, Y. G. Li, *J. Am. Chem. Soc.* **2009**, *131*, 15586; [5c] H. Zhou, L. Yang, S. C. Price, K. J. Knight, W. You, *Angew. Chem., Int. Ed.* **2010**, *49*, 7992; [5d] C. Piliego, T. W. Holcombe, J. D. Douglas, C. H. Woo, P. M. Beaujuge, J. M. J. Fréchet, *J. Am. Chem. Soc.* **2010**, *132*, 7595; [5e] Y. Liang, Z. Xu, J. Xia, S.-T. Tsai, Y. Wu, G. Li, C. Ray, L. Yu, *Adv. Mater.* **2010**, *22*, E135; [5f] H.-Y. Chen, J. Hou, S. Zhang, Y. Liang, G. Yang, Y. Yang, Y. Wu, G. Li, *Nat. Phot.* **2009**, *3*, 649.

[6] J. Hou, M.-H. Park, S. Zhang, Y. Yao, L.-M. Chen, J.-H. Li, Y. Yang, *Macromolecules* **2008**, *41*, 6012.

[7] Y. Zou, A. Najari, P. Berrouard, S. Beaupré, B. R. Aïch, M. Leclerc, *J. Am. Chem. Soc.* **2010**, *132*, 5330.

[8] [8a] N. Blouin, A. Michaud, D. Gendron, S. Wakim, E. Blair, R. Neagu-Plesu, M. Belletête, G. Durocher, Y. Tao, M. Leclerc, *J. Am. Chem. Soc.* **2008**, *130*, 732; [8b] C. V. Hoven, X. Dang, R. C. Coffin, J. Peet, T.-Q. Nguyen, G. C. Bazan, *Adv. Mater.* **2010**, *22*, E63; [8c] J. C. Bijleveld, M. Shalid, J. Gilot, M. M. Wienk, R. A. J. Janssen, *Adv. Funct. Mater.* **2009**, *19*, 3262.

[9] Y. F. Li, Y. Cao, J. Gao, D. L. Wang, G. Yu, A. J. Heeger, *Synth. Met.* **1999**, *99*, 243.

[10] GADDS V4.1.14 "*General Area Detector Diffraction System Program for Instrument Control and Data Collection*" BRUKER AXS Inc., Madison, WI.

[11] EVA V8.0 "*Graphics Program for 2-dimensional Data evaluation and Presentation*" BRUKER AXS Inc., Madison, WI.

[12] [12a] R. C. Coffin, J. Peet, J. Rogers, G. C. Bazan, *Nat. Chem.* **2009**, *1*, 657; [12b] F. Galbrect, T. W. Bünnagel, U. Scherf, T. Farrell, *Macromol. Rapid Commun.* **2007**, *29*, 387.

[13] [13a] J. Peet, N. S. Cho, S. K. Lee, G. C. Bazan, *Macromolecules* **2008**, *41*, 8655; [13b] L. M. Chen, Z. Hong, G. Li, Y. Yang, *Adv. Mater.* **2009**, *21*, 1434.

[14] [14a] G. Li, Y. Yao, H. Yang, V. Shrotriya, G. Yang, Y. Yang, *Adv. Funct. Mater.* **2007**, *17*, 1636; [14b] Y. Zhao, Z. Xie, Y. Qu, Y. Geng, L. Wang, *Appl. Phy. Lett.* **2007**, *90*, 043504.

[15] J. S. Moon, C. J. Takacs, S. Cho, R. Coffin, H. Kim, G. C. Bazan, A. J. Heeger, *Nano Lett.* **2010**, *10*, 4005.